

Key Injury Regions for Passenger Car Drivers in Frontal Crashes: A Comparison of Results from IGLAD and Finite Element Simulations using a Human Body Model

Felix Ressi, Desiree Kofler, Wolfgang Sinz, Ernst Tomasch, Corina Klug

Abstract Identifying the key injury regions of vehicle occupants is an important step to further improve the safety of future vehicles. Their estimation for occupants of future vehicle concepts with novel restraint strategies poses a particular challenge. While accident databases can offer valuable insights, they are limited to the current vehicle fleet. Human body models (HBMs) are an interesting alternative, since they enable the investigation of injury mechanisms and the estimation of effects of changing boundary conditions and protective countermeasures. To produce reliable results though, these models need to be set up with representative boundary conditions and reliable injury predictors have to be identified.

As a first step, the present study tried to match the relative injury frequency across all body regions observed in a real-world accident database sample to simulation results obtained with a detailed HBM. The occupant model was seated in a simplified vehicle model and variability in the vehicle fleet was accounted for by varying loads, boundary conditions and restraint system parameters.

Differences between the predicted frequencies of injury were identified – most prominently for the head. Since this method can be seen as a plausibility check for the human body model, thresholds for the strain-based assessment are discussed.

Keywords accident data analysis, human body modelling, injury regions, occupant safety

I. INTRODUCTION

Globally, passenger car occupants account for about a third of all road traffic fatalities [1]. They make up 48% of road traffic fatalities in Europe and even 64% in the USA [1]. According to the Insurance Institute for Highway Safety, at least 56% of fatalities in passenger car crashes occur in frontal crashes [2]. Comprehensive legislation and New Car Assessment Programmes (NCAPs) in particular, with their even higher demands on vehicle safety, have driven many improvements in passive occupant safety. To make future cars even safer, the identification of the key injury regions can offer valuable insights, for regulatory bodies as well as for car manufacturers.

One way to assess these relevant injury regions is the analysis of in-depth accident databases, which connect detailed accident data with injury data on collision participants. Many prior studies analysed data from the United States' National Automotive Sampling System Crashworthiness Data System (NASS-CDS) to analyse injury risk. For frontal crashes, the body regions with the highest AIS2+ injury risks at 56 km/h were identified to be the lower extremities (25%), the upper extremities (16%), the thorax (12%) and the head (8%) if the seat belt was used [3–4]. They also investigated the influence of different model years of passenger cars on injury risk. NASS-CDS data also allows modelling the effects of various factors on injury risks. An example is the evaluation of the relative impact of age, body mass index and gender on AIS3+ injury risk. Age was identified to have the largest effect on injury risk. This applies to all crash modes and particularly to the head and thorax regions. [5]

Detailed finite element human body models (FE HBMs) are powerful tools to further understand injury mechanisms as well as improve and assess safety measures. [6]

The combination of real-world accident data with detailed FE HBM simulations offers the possibility to change simulation parameters and estimate the effects on real-world outcomes. [6–7] recreated *individual* cases from the Crash Injury Research and Engineering Network (CIREN) database in-silico, i.e., in computer simulations, with a detailed FE HBM. Subsequent variation of selected input parameters was performed to improve the understanding of the effect size on injury prediction [6].

Felix Ressi (+43 316 873 30363, felix.ressi@tugraz.at) and Desiree Kofler are Research Assistants, Wolfgang Sinz is Associate Professor, Ernst Tomasch is Senior Researcher and Corina Klug is Assistant Professor at the Vehicle Safety Institute at Graz University of Technology in Austria.

This approach of validating a simulation model with accident data has also been adopted by researchers who developed a generic vehicle interior model and used an HBM to evaluate injuries to the thorax. However, the validation was not based on individual cases, but on a large sample of accidents from NASS/CDS. They referred to the concept as *population based validation*. Since they focussed on thoracic injuries, the effects of vehicle or restraint parameters on other body regions were not addressed in their research. [8–9]

While focussing on pedestrians instead of car occupants, [10] also combined accident data with simulation models to estimate the effects of parameter changes on injuries. By drawing on detailed accident data, the authors defined a Virtual Test System (VTS). They investigated different simulation test samples for multi-body simulations in MADYMO, i.e., sets of simulations with certain parameter ranges, to compare how well these individual sets represent the real-world pedestrian crashes.

The present study is a first step towards a form of VTS for passenger car drivers in frontal crashes. By using a vehicle interior with all relevant restraint systems and adequate ranges of input parameters for this model, the results should be representative of the outcome of real-world crashes. The aim was to compare the key injury regions from a set of real-world accidents with results from FE HBM simulations with varying boundary conditions. In addition, currently available assessment criteria have been checked for plausibility.

II. METHODS

In order to identify the key injury regions of male drivers of passenger cars in frontal collisions, data from a global accident database were analysed. The simulations with a 50th percentile male FE HBM were set up with delta-v values corresponding to the filters applied to the accident database cases and analysed using strain-based injury criteria. The goal was not to model individual cases from the sample but to vary input parameters in such a way that the overall results would be comparable. Finally, the results of both approaches (accident data analysis and FE HBM simulations) were compared and discussed. Fig. 1 shows a flow chart of the approach.

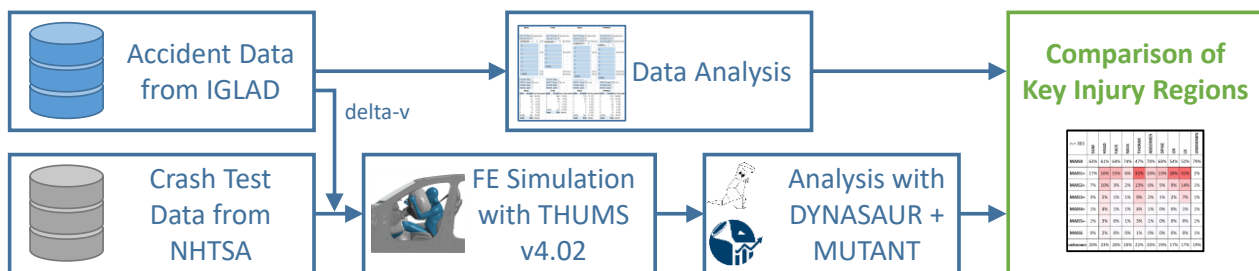


Fig. 1. Flow chart of the method used in the present study.

Accident Data Analysis

The analysis was conducted with a data set of the Initiative for Harmonisation of Global In-depth Traffic Accident Data (IGLAD) [11]. The goal of the initiative is to set up an international in-depth accident database. To achieve this, a common data scheme was defined for all participating databases, which enables to merge the different data samples into one. [12] The data set used in the present study consisted of 4,943 accidents from 2013 to 2017. It was filtered for male drivers of passenger cars involved in frontal accidents with known change in velocity due to the collision (delta-v) and a principal direction of force (PDOF) of 0°. This is equivalent to a force direction of 12.00 according to the Collision Deformation Classification (CDC) SAE J224 [13]. In addition, cases with secondary collisions were not considered. Collisions with vulnerable road users and animals as well as cases in which the opponent had not been specified were also excluded. Five cases were eliminated from the sample individually due to implausible data (two delta-v values, but only one collision coded). The cases were filtered further to exclude cases where delta-v was below the test data available for the finite element simulations with the FE HBM. Therefore, only cases with delta-v values of 28 km/h and above were included in the final analysis. This also represented the median delta-v of all cases with Maximum Abbreviated Injury Scale (MAIS) 1 injuries. Cases with delta-v above 64 km/h were also excluded. This threshold was chosen since it represents the maximum delta-v found in the crash test data, which was used as input for the simulations. Higher delta-v values than those resulting from common legislation and consumer crash tests were likely to result in significant safety cell deformations. These high severity crashes were not considered in this study. Therefore, the filters were adjusted

to also exclude cases with deformation into the passenger compartment (filter set to only include CDC deformation extent ≤ 5) and small overlap crashes (filter set to exclude CDC specific longitudinal location of deformation codes L0 and R0).

Since the results of the accident data analysis focus on the injury assessment, an overview of the data structure is given in this section.

The filtering resulted in 124 cases from 11 countries. European accident databases accounted for $\frac{2}{3}$ of these cases and Asia for 15%. The rest came from the US (13%) and Australia (6%). Fig. A-1 illustrates this distribution, while Fig. A-2 shows the distribution of the source countries for the complete unfiltered IGLAD sample.

As can be seen in Fig. A-3, in the majority of collisions (72%), the opponent was a passenger car or a sport utility vehicle (SUV). In 6% of the cases, the car collided with a bus or a truck, while vans and light trucks only accounted for 5% of collision opponents. The rather large portion of 17% of *other* opponents is made up of poles, trees, traffic lights, actual roadside, guardrails or walls.

Occupant weight and height were available for 50 and 48 cases, respectively. The average height was 177 cm, (SD=6.9) and the average mass 86.6 kg (SD=16.7).

The age distribution of the 112 cases, where driver age was available, is shown in Fig. 2. Drivers who were 30 years old or younger accounted for 32% of all cases. Those between 30 and 50 years of age make up 35% and the group between 50 and 70 years represents 21%. Only 13% were older than 70 years. For a better overview, the distributions of driver age, height and weight are provided as box plots in Fig. 3.

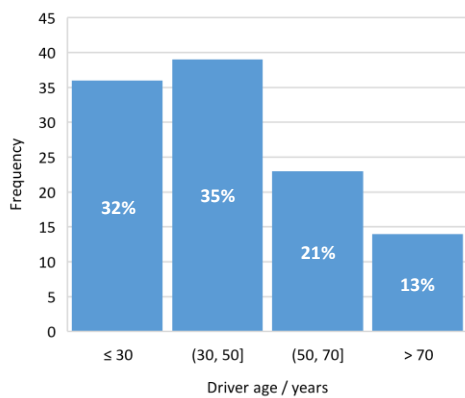


Fig. 2. Age distribution in the IGLAD sample when filtering for male car drivers in frontal collisions with delta-v 28 - 64 km/h categorised into four groups (n=112).

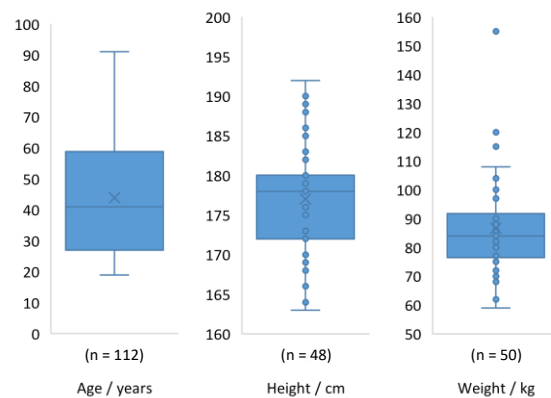


Fig. 3. Box plots of driver age, height and weight in the IGLAD sample when filtering for male car drivers in frontal collisions with delta-v 28 - 64 km/h.

For each individual case, the maximum AIS injury level for each body region (MAIS) according to AIS90 Update 98 was known [11]. While MAIS is often associated with the most severe injury to the *whole body*, the use of MAIS on a *body region level* is also widely used [14]. Accordingly, there were eight MAIS values for each of the 124 cases (1,116 in total): one for each of the seven AIS body regions, i.e. head, face, neck, thorax, abdomen, spine, upper extremities, lower extremities and one additional *unknown* category (these regions represent the columns in Fig. 5).

Finite Element Simulations

The FE simulations were performed using LS-Dyna mpp R9.2.0 single precision on an Intel Xeon 64bit-based high performance computing cluster running a Linux operating system. Each simulation was run on two computing nodes with 20 processors each. The vehicle model was based on a state-of-the-art occupant safety model of an executive saloon car. To reduce complexity and increase calculation speed, the model was simplified. Most of the components in the interior were originally constructed of many intricate sub-parts. These were merged into larger parts and their geometries were simplified. In addition, the body in white (BIW) was modelled as a rigid part. Because there was no door or side window in the original model, a generic door with a rigid side window was included. While the resulting simplified model was not validated as such, test simulations with the original crash pulse were made to ensure comparable behaviour to the original version. In addition, since the

model in this study is not supposed to represent one particular vehicle but rather work as a generic model, validation requirements are more general.

The restraint system consisted of a seat, a three-point seatbelt with pretensioner and load-limiter, a collapsible steering column, steering wheel and airbag as well as a knee airbag. These components were not modified. The range of variation for the restraint system parameters is listed in Table I. Since it was not the goal of the present study to model each accident from the IGLAD sample individually, but to find a set of parameters, which represent the sample, crash pulses from different vehicles were chosen. They were derived from the publicly available National Highway Traffic Safety Administration (NHTSA) Vehicle Crash Test Database [15].

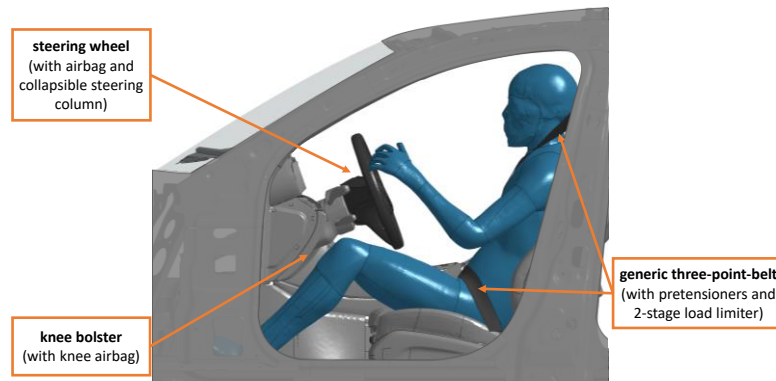


Fig. 4. Side view of the FE model with the positioned THUMS v4.02 AM50.

The acceleration signals from five full overlap rigid wall crash tests with initial velocities between 24 and 56 km/h were taken from the database. These were filtered with a low pass filter (CFC60) and integrated to obtain the velocity-time curves. The exact initial velocity was also taken from the database and applied to the whole simulation model. To simulate the crash loads on the occupant, the velocity-time curves were applied to the rigid BIW as a prescribed motion. This method is equivalent to a sled test configuration, where the BIW is mounted on a rigid sled, which is decelerated to simulate crash loads. The velocity time-history curves of the crash pulses used in this study are shown in Fig. A-4.

Based on these time-history curves, the deployment times or times-to-fire (TTF) for the irreversible restraint systems, i.e. belt pretensioners and airbags, were estimated. Since the actual algorithms are proprietary, a simple algorithm was implemented. It was based on a deceleration threshold of 9.81 ms^{-2} for activation and a subsequent integrated distance limit for the actual deployment. Because the TTF were also varied, the times derived with this algorithm did not necessarily need to represent the probable real-world deployment times. Nevertheless, a description of the algorithm can be found in the appendix.

TABLE I
OVERVIEW OF INPUT PARAMETER RANGES FOR THE FE HBM SIMULATIONS

Parameter	Units	Min.	Max.
<i>TTF1</i>	ms	6.77	20.85
<i>TTF2</i>	ms	11.77	25.85
<i>Shoulder belt force limit</i>	kN	3.8	6.0
<i>Second load limiter switch</i>	-	0	1
<i>KAB on/off switch</i>	-	0	1
<i>DAB vent diameter</i>	mm	25	50
<i>Steering Column Force</i>	kN	3.8	6.0
<i>Friction between DAB and THUMS</i>	-	0.1	0.4

Based on the calculated TTF for each crash pulse, the seat belt pretensioner at the retractor side was triggered first (TTF1 in Table I). With a delay of 5 ms, the other restraint systems, i.e., anchor pretensioner and airbags, were deployed (TTF2 in Table I). Since the real-world deployment times were not known for the crash pulses and

because they are individual for every vehicle, the baseline TTF was varied in two additional steps. One *early deployment* scenario, where the times were shifted by -3 ms, and a late deployment scenario, for which the times were delayed by +5 ms.

Beside the TTF, other parameters for the restraint systems were also varied to account for the multitude of different vehicles found in the IGLAD data. Table I sums up these parameters and their range of variation.

The shoulder belt force limiter was set to values between 3.8 kN and 6 kN. For some simulations, a second lower load limiter level was activated 30 ms after TTF1. In addition, the knee airbag (KAB) was deactivated for some variants. The driver airbag (DAB) vent hole diameter was varied between 25 mm and 50 mm, which is equivalent to a 4-fold increase of the vent area. The force required to move the telescopic steering column was varied in a range between 3.8 kN and 6.0 kN. In addition, to account for different airbag materials, the coefficient of friction between the occupant's head and the airbag was lowered from 0.4 to 0.1 in some simulation runs. These parameter ranges are in accordance with values found in literature [8–9].

In the present study, the individual simulations were not defined by combining parameters based on pseudo random sampling methods (i.e. Latin hypercube sampling [9]). Instead, 13 variants were defined for each of the five crash pulses. For these variants, the parameters were selected to cover a variety of vehicles and restraint systems. The restraint systems in the model represent a high state-of-the-art standard of occupant safety. To account for vehicles with a lower standard (in particular older model years), some combinations which, according to the data presented in [9], are still within reasonable limits, but are less likely to be found in contemporary vehicles, were added. Table A-I lists an overview of these variants. Additionally, two variants with a PDOF of +15° and -15° instead of 0° were added for each crash pulse. By including these, the simulation matrix accounts for the fact that PDOF angles up to ±15° are likely to be coded as 0° in most real-world accident reconstructions. As a result, this should improve the representativeness of the HBM simulations. The other parameters in these two variants were kept identical to the *baseline* (variant 1), as can also be seen in Table A-I.

The resulting 75 individual cases covered a delta-v distribution very similar to that of the IGLAD sample. Fig. A-5 shows box plots of the two delta-v ranges. The 75 variants were then prepared and simulated with LS-Dyna. All simulations were completed successfully and analysed in detail. The complete simulation matrix is presented in Table A-II.

A THUMS v4.02 AM50 was used to model the driver. The model has been validated extensively on component and regional level as well as in whole body load cases. [16] The height of this HBM (178.6 cm) deviates by less than 1% from the average driver height in the real-world accidents (177 kg) while the weight of the HBM (77.3 kg) is about 12% lower than the average driver weight in the IGLAD cases (86.6 kg). Positioning of the HBM was based on a reference position of a Hybrid III 50th percentile male anthropomorphic test device (ATD). The ATD was included in the base model and originally positioned according to FMVSS 208 [17]. The undeformed seat was deformed accordingly in a separate simulation. The hands were not positioned directly on, but next to the steering wheel (see Fig. A-6 and Fig. A-7). While this will affect arm kinematics, the effects are expected to be negligible. Since the THUMS v4.02 is a passive model, not capable of *gripping* the steering wheel, even when the fingers are placed around the rim, they would slide off with little resistance. Unlike the parameters listed in Table I, the seat position and the seated position of the HBM were kept constant for all simulations. Fig. 4 shows the entire model including the positioned HBM.

The HBM simulation outputs were analysed using the open-source post-processing tools DYNASAUR [18] and MUTANT [19]. Table II lists the injury metrics and the associated AIS severity used for the present study with respect to the AIS body regions also used in the accident analysis.

Brain injuries were estimated by evaluating maximum principal strain (MPS) of finite element brain elements. When the 95th percentile of the MPS (MPS95) exceeded 0.3, AIS2+ brain injury was assumed. Similarly, injury was assumed, if MPS99 in the elements of cortical bones or internal organs exceeded the respective strain threshold. These metrics were applied to all body regions listed in Table II.

The limits for bone fracture were based on a publication which compared literature on age effects on failure strain for cortical bones [7]. The FE HBM outputs were evaluated with respect to four strain limits, which corresponded to the four age groups in the IGLAD dataset depicted in Fig. 2. These results were then combined to reflect the relative frequency of each of the four age groups in the sample. The ribs were also evaluated for the four age groups utilising the empirical cumulative distribution derived in [20]. Since this distribution is based on a binomial probability model, the total number of fractured ribs in all simulations can be estimated to be the

sum of the individual rib fracture risks of all simulations. This rib evaluation was performed for the risk of one fractured rib as well as for two fractured ribs. According to the 98 Update of the 1990 Abbreviated Injury Scale (which is the basis for the IGLAD coding), the fracture of one rib can be associated with minor or serious injuries (AIS severity 1 or 3), depending on whether there is also hemo- or pneumothorax present [21]. For the same reason, two rib fractures can be associated with an AIS2 or AIS3 injury. For the present paper, AIS2 injury was only assumed if fracture was predicted in at least two ribs.

TABLE II
INJURY METRICS FOR THE FE HBM SIMULATIONS

AIS region	Body region		Strain limit	Literature source	Associated AIS severity
1	Head	Brain	30%	[22]	2+
		Skull	1.57% - 3.73%	[7]	3+
3	Neck	C1 – C7	1.57% - 3.73%	[7]	3
4	Thorax	Ribs	-	[20]	1-3+
		Heart	30%	[22]	3+
5	Abdomen	Liver, Spleen	40%	[22]	2-3+
6	Spine	T1 – T12, L1 – L5	1.57% - 3.73%	[7]	3
7	Upper extr.	Ulna, Radius, Humerus	1.57% - 3.73%	[7]	2-3
8	Lower extr.	Pelvis	1.0%	[23]	2-3
		Femur	1.57% - 3.73%	[7]	3
		Tibia, Fibula	1.57% - 3.73%	[7]	2-3

In addition, pelvic fractures were predicted according to [23], who found a strain threshold of 1% to be in good agreement with a criterion predicting pelvic fractures, albeit under lateral loading. Injuries to the face (AIS region 2) were not assessed in the HBM simulations due to a lack of injury metrics.

Associating a single AIS severity score to finite elements exceeding a threshold value for maximum principal strain is a simplification. In theory, no exact AIS code (or severity) can be associated without detailed knowledge of the exact injury, i.e. open or closed fracture, estimated amount blood loss, etc. In the present study a value of AIS2 or higher (if higher severity injuries exist) has been assumed. For the body regions considered here, this is a conservative estimation.

III. RESULTS

Accident Data Analysis

The results from the IGLAD analysis for injuries up to MAIS3+ are illustrated in Fig. 5. Results for all injury severities are available in Fig. A-9 and Fig. A-10. Of the total 1,116 MAIS values in the data set, only 170 represent injuries (MAIS1+). Fig. 6 facilitates the evaluation of relative frequency of injuries in the sample, as the values are given as ratios with respect to the total number of drivers (124). Only the first column *sum* represents the ratio of the total amount of respective MAIS injuries as a ratio to the total number of 1,116 MAIS values. In both figures, darker background colours indicate higher values. In terms of general injury frequency, MAIS1+ injuries to the thorax, upper and lower extremities are most prevalent. Of the 124 drivers in the IGLAD cases, 8% suffered MAIS2+ injuries to the thorax. In 6% and 5% of the cases, the head and the upper extremities were injured with a severity of MAIS2+. In terms of MAIS3+ injuries, only 15 injuries were observed. Five of these injuries affected the thorax, in four cases, the head and the lower extremities were injured and one case affected the abdomen.

n = 124	SUM	HEAD	FACE	NECK	THORAX	ABDOMEN	SPINE	UX	LX	UNKNOWN
MAIS0	792	89	91	102	61	101	92	72	79	105
MAIS1+	170	11	17	7	39	8	17	37	30	4
MAIS2+	37	7	1	1	10	2	4	6	5	1
MAIS3+	15	4	0	0	5	1	0	0	4	1

Fig. 5. Number of MAIS0 to MAIS3+ injuries for each body region based on the filtered IGLAD sample (male drivers, frontal collisions, delta-v 28 - 64 km/h).

n = 124	SUM	HEAD	FACE	NECK	THORAX	ABDOMEN	SPINE	UX	LX	UNKNOWN
MAIS0	71%	72%	73%	82%	49%	81%	74%	58%	64%	85%
MAIS1+	15%	9%	14%	6%	31%	6%	14%	30%	24%	3%
MAIS2+	3%	6%	1%	1%	8%	2%	3%	5%	4%	1%
MAIS3+	1%	3%	0%	0%	4%	1%	0%	0%	3%	1%

Fig. 6. Relative injury frequency for each body region with respect to MAISx+ injury severity in percentage based on the filtered IGLAD sample (male drivers, frontal collisions, delta-v 28 - 64 km/h).

Finite Element Simulations

A time series of an exemplary simulation (ID 055, delta-v = 28 km/h) is shown in Fig. 7. All 75 simulations finished with normal terminations and their results were then analysed.

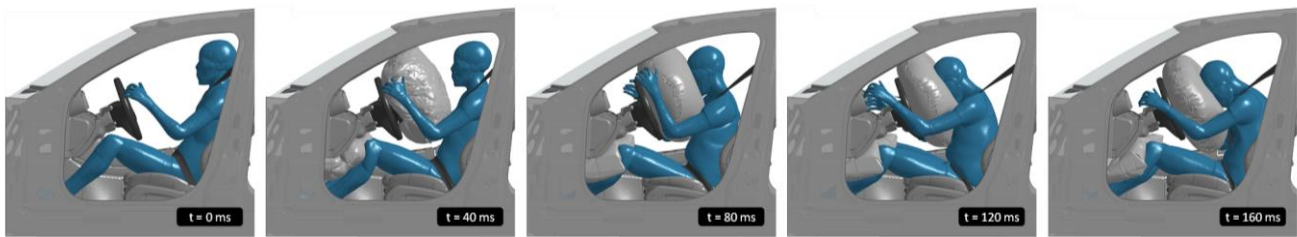


Fig. 7. Time series of simulation ID055 in 40 ms increments (simulation matrix listed in Table A-II for details).

The predicted relative injury frequencies from the FE simulations were quite different to the ones derived from the real-world accidents. Fig. 8 illustrates the results for the FE HBM using the injury metrics listed in Table II, while Fig. 9 presents the IGLAD results in the same format.

n = 75	SUM	HEAD	FACE	NECK	THORAX	ABDOMEN	SPINE	UX	LX	UNKNOWN
MAIS0+	57%	5%	-	100%	0%	0%	97%	100%	97%	0%
MAIS2+	43%	95%	-	0%	100%	100%	3%	0%	3%	0%
unknown	0%	0%	-	0%	0%	0%	0%	0%	0%	0%

Fig. 8. Predicted relative injury frequency for each HBM body region with respect to the MAIS0-1 and MAIS2+ severities as percentage (limits from literature).

n = 124	SUM	HEAD	FACE	NECK	THORAX	ABDOMEN	SPINE	UX	LX	UNKNOWN
MAIS0-1	83%	75%	86%	87%	73%	86%	85%	83%	84%	87%
MAIS2+	3%	6%	1%	1%	8%	2%	3%	5%	4%	1%
unknown	14%	19%	13%	12%	19%	12%	12%	12%	12%	12%

Fig. 9. Relative injury frequency for each body region for the filtered IGLAD sample to facilitate the comparison to the FE HBM results.

Only MAIS2+ injuries were considered. The main reason for this is the lack of a complete range of injury risk curves for all body regions and severity levels. Additionally, MAIS3+ injuries are quite rare in the IGLAD sample. Of the 1,116 MAIS values for the 124 drivers in the sample only 15, or 1%, represented serious injury or worse (MAIS3+). For the 75 FE simulations, this would translate into about seven MAIS3+ injuries. When these are categorised further into the seven considered body regions, statistical analyses bear limited value.

Thoracic and abdominal MAIS2+ injuries are predicted to occur in all simulated cases. For the majority of cases (95%) also moderate or worse injuries to the head are predicted. The relative frequencies for MAIS2+ injuries to the neck and the upper extremities are zero, while the spine and lower extremities are injured in 3% of the simulations. All these predictions are based on the injury metrics listed in Table II.

The boxplots in Fig. 10 and Fig. 11 illustrate the range of values for the maximum principal strains of selected organs and cortical bones in the spinal column, which were the basis of the injury assessment. It is obvious from looking at the values for the soft tissue strains in Fig. 10 that the MPS95 were above the respective limits of 0.3 and 0.4 (listed in Table II) in all 75 simulations. The MPS95 of three exemplary vertebrae shown in Fig. 11 were all below the threshold of 1.5%, with the exemption of one simulation in which the 12th thoracic vertebra exceeded it by a small margin.

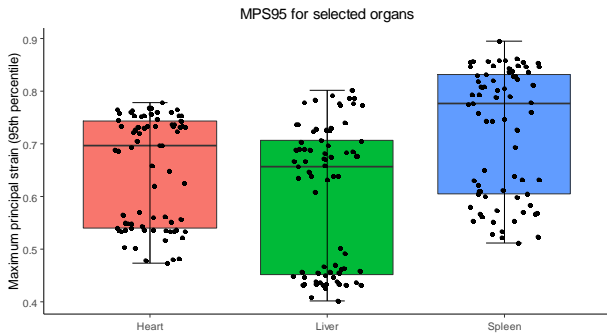


Fig. 10. 95th percentile maximum principal strains of exemplary organs (n = 75).

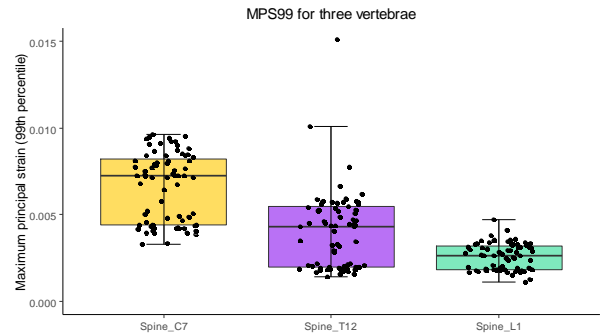


Fig. 11. 99th percentile maximum principal strains of exemplary cortical bones in the spine (n = 75).

The relative frequency of thoracic injuries was dominated by the strains of the heart, while the number of cases with predicted rib fractures (≥ 1) in the sample was 4.4. Fig. 12 and Fig. 13 illustrate how this number is calculated from the predicted number of cases with fractured ribs for each age group.

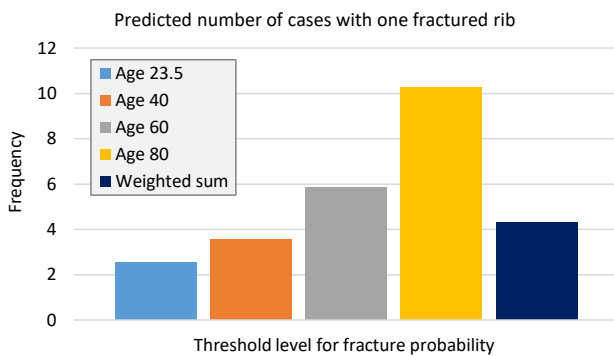


Fig. 12. Predicted number of cases with one fractured rib.

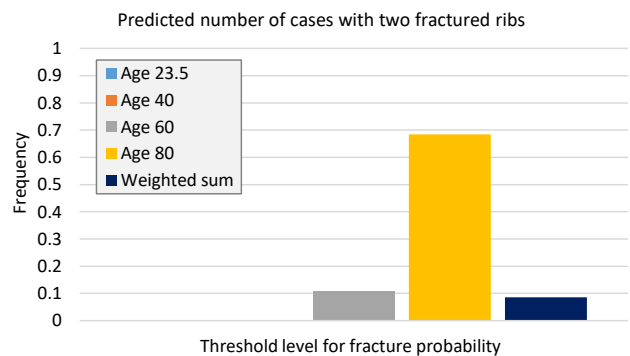


Fig. 13. Predicted number of cases with at least two fractured ribs.

The four bars on the left-hand side in Fig. 12 represent the number of cases with one rib fracture for each age group – assuming that all 75 simulations are evaluated for this individual age group. The fifth bar, labelled *Weighted Sum*, is the sum of these numbers multiplied with the relative frequency of each age group according to the IGLAD sample (as illustrated in Fig. 2). This results in a prediction of 4.3 cases with one fractured rib. While Fig. 12 shows the number of cases where *one* fractured rib is predicted, Fig. 13 illustrates the number of cases associated with *two* fractured ribs. Even in the age groups of 60 and 80 years, less than one case with two fractured ribs is predicted. The weighted sum of cases associated with two fractured ribs is only 0.1.

IV. DISCUSSION

The results of the IGLAD analysis identified the thorax, the head and the upper extremities as the three key injury regions when considering MAIS2+ injuries. Similar studies found the lower extremities to be more frequently injured than the upper extremities [3–4]. This discrepancy can be explained with the filter criteria used for the IGLAD data. They were aimed to eliminate any cases with intrusion into the passenger compartment, which explains the lower prevalence of injuries to the lower extremities compared to the head and the thorax. Due to the very selective filtering applied to the accident data, the remaining sample was made up of 124 cases.

While in statistical analyses, larger sample sizes are always favourable, the filter criteria were chosen in an effort to improve consistency between the accident database analysis and the simulations.

Assuming the FE simulations themselves are representative of the IGLAD sample, the results overestimated the prevalence of injuries in the head, the thorax and the abdomen. In an effort to investigate this in more detail, the injury metrics were re-evaluated and alternative metrics and thresholds were analysed.

First, the head injury metrics were compared to commonly used kinematic injury criteria. Table III compares the relative frequency of head injuries in the IGLAD dataset to the predicted frequency according to risk curves for AIS2+ injury for HIC₁₅ [24] and the Brain Injury Criterion (BrIC) [25] for the FE HBM simulations. In addition, the mean values of the injury criteria are given. The prediction of zero head injuries based on HIC₁₅ can probably be attributed to the fact that it only evaluates linear accelerations. This was one of the main motivations behind developing BrIC [25], which, contrary to HIC₁₅, seems to overestimate the prevalence of head injuries in the current analyses. Table III also shows that the relative injury frequency based on MPS95 is even higher than the one based on BrIC.

TABLE III
COMPARISON OF THE RELATIVE FREQUENCY OF MAIS2+ INJURIES OF THE HEAD

Data source/injury metric	rel. frequency	Mean of injury criterion
<i>IGLAD</i>	6%	-
<i>FE HBM based on HIC₁₅</i>	0%	152
<i>FE HBM based on BrIC</i>	60%	0.594
<i>FE HBM based on MPS95</i>	95%	0.644

Since the injury risk curves for BrIC are based on risk curves for the Cumulative Strain Damage Measure (CSDM) and MPS of two FE head models [25], the predictions by MPS and BrIC are expected to correlate. As a weak correlation was observed in the first evaluations, using the entire simulation duration (Fig. 15 left), additional analyses were performed. To compare the correlation for the 75 simulations listed in Table A-II, BrIC and MPS95 were evaluated for three different time ranges. Fig. 14 illustrates the chosen evaluation times t_1 and t_2 for one exemplary simulation.

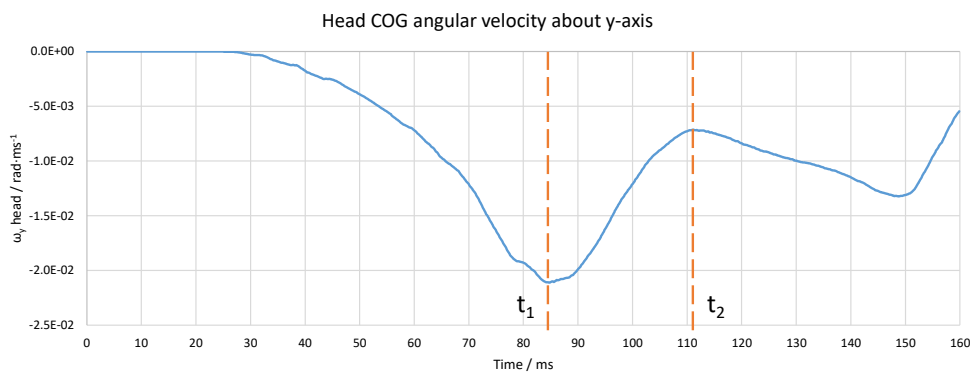


Fig. 14. Exemplary time-history curve of the angular velocity of the head centre of gravity for simulation ID125 to illustrate the evaluation times t_1 and t_2 .

The first peak of the angular velocity about the y-axis of the centre of gravity in the head of the HBM has been chosen as t_1 . The next local peak is chosen for deriving t_2 . Evaluations using the whole simulation time are marked with t_{End} . These times were evaluated for each simulation individually. Fig. 15 shows plots of BrIC values over the corresponding MPS95 values of all simulations for these three evaluation time ranges.

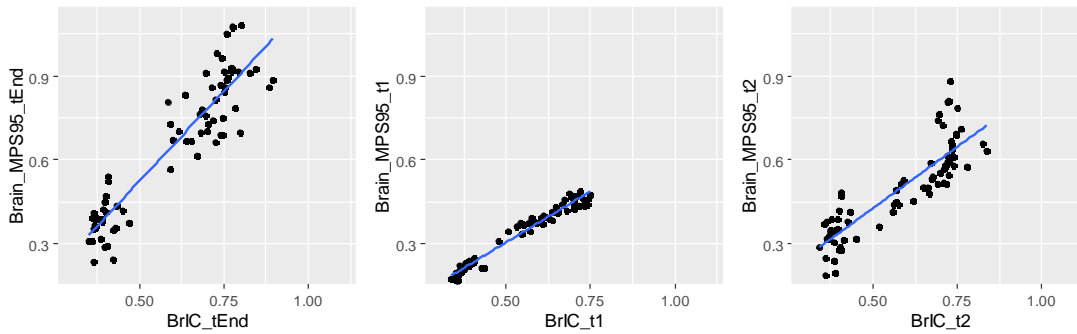


Fig. 15. Correlation between BrIC and MPS95 for all simulations when evaluating the entire simulation t_{End} , until the first peak of angular velocity t_1 and the following local peak t_2 (see example in Fig. 14).

The plot on the left is based on an evaluation of the entire simulation time (t_{End}). At $R^2 = 0.85$, the correlation between BrIC and MPS95 is considerably lower than reported in [25] ($R^2 = 0.98$). When the simulation is only evaluated until the first peak of the angular velocity (t_1), the correlation improves dramatically ($R^2 = 0.96$). Evaluating until the following local peak (t_2) gives a lower R^2 compared to the entire simulation time ($R^2 = 0.76$). One explanation for the better correlation for the evaluation until t_1 might be the way BrIC has been defined. Since it only considers the absolute maximum rotational velocity in each direction, evaluating the simulation after this maximum was reached, does not change the BrIC value. In the simulations at hand, BrIC was dominated by the rotational velocity about the y-axis. Therefore, evaluating the simulation after the peak value of this angular velocity has been reached, does not affect BrIC considerably.

A recent study found that comparable head injury levels between real-world accidents and simulations could be obtained when ensuring similar values for PDOF in the two data sources. [26] In the present study, the IGLAD sample was filtered to only include cases with a PDOF of 12.00 (0°), with the next available groups in the filter criteria being 11.00 and 01.00 (i.e. $\pm 30^\circ$). To account for this uncertainty in the simulations, 87% were simulated with a PDOF of 0° , 6.5% with $+15^\circ$ and -15° respectively. Assuming that the PDOF in real-world collisions is hardly ever exactly 0° (certainly in less than 87% of all cases), the head injury risk predicted in the simulations should be *lower* than in the real-world accidents.

Using the MPS95 values until t_1 (MPS95_ t_1), the relative frequency of AIS2+ injuries predicted by the FE HBM decreased to 62%, which is still much higher than the 11% observed in the IGLAD analysis. To the best knowledge of the authors, there are currently no published injury risk curves (IRCs) for brain injury for the THUMS v4.02.

As a first estimation, the IRCs published by [25], which have not been validated against the brain model used in THUMS v4.02, were used to estimate the threshold value for MPS95 related to a 50% AIS2+ risk. The MPS threshold to predict MAIS2+ injury would then increase to 0.45. With this threshold level, the predicted injury prevalence from the FE HBM reduces to 13%, which is still twice as much compared to the relative frequency observed in the IGLAD dataset, as can be seen in Fig. 16. An overview on the discussed strain limits is presented in Fig. 17.

	SUM	HEAD	FACE	NECK	THORAX	ABDOMEN	SPINE	LX	LX	UNKNOWN
MAIS2+ IGLAD	3%	6%	1%	1%	8%	2%	3%	5%	4%	1%
MAIS2+ FE HBM	43%	95%	-	0%	100%	100%	3%	0%	3%	0%
MAIS2+ FE HBM adjusted	3%	13%	-	0%	1%	3%	3%	0%	3%	0%
difference adj. FE HBM - IGLAD	0%	8%	-	-1%	-7%	1%	-1%	-4%	-1%	-1%

Fig. 16. Relative injury frequency for each body region with respect to MAIS2+ injury severity in percentage for adjusted limits to match the IGLAD sample better.

Maximum principal strains for strain-based assessment	Brain	Heart	Liver, Spleen	Age dependent limits for cortical bones			
				23.5	40	60	80
Limit from literature	0.3	0.3	0.4	0.0373	0.0310	0.0233	0.0157
Adjusted Limit	0.45	0.8	0.86	-	-	-	-

Fig. 17. Overview of the adjusted limits for the strain-based assessment criteria. Also the 95th percentile strains have been used instead of the 99th for all organs.

The overestimation of head injury risk by evaluating maximum principal strains underlines the need for further research in this area. In a study focussing on the prediction of severe head injuries for VRUs, MPS was found to perform well [27]. This could point to issues with the IRCs for injuries of lower severity, as we focussed on AIS2+ injuries. A recent study suggested that the overestimation might also be caused by the constitutive model used in the brain of the THUMS v4.02 [28]. They conclude that using an Ogden hyperviscoelastic model could improve prediction of brain deformation and the associated strains [28]. It should be noted though, that the injury estimation could certainly be improved by using validated model specific IRCs – if they were available.

To get a more robust strain value for the abdominal organs, the MPS95 strains were evaluated instead for the 99th percentile (these are shown in Fig. 10). While improving robustness, this still led to a predicted relative injury frequency of 100% for the abdomen. The relative frequency of abdominal injury from the IGLAD analysis could only be matched by raising the MPS95 threshold to 0.86 (results are shown in Fig. 16), which seems implausibly high and therefore should be the subject of further research.

Similar to the high strains in the liver and the spleen, the thoracic injuries were dominated by the 99th percentile strains from the heart, while the sum of the fracture risks for two ribs, weighted by the age distribution in the IGLAD sample (mean age: 44 years), was only 0.1, which translates to a relative frequency of only 0.1%. This suggests that injury to the heart is overestimated, not least because the load cases used for the simulations are standard crash tests, in which reducing the injury severity is a design objective for vehicle manufacturers. Evaluating the 95th instead of the 99th strain percentile for the heart did not change the relative injury frequency for the thorax. By increasing the threshold strain for the heart to 0.8, a thoracic injury frequency of 1% was predicted (shown in Fig. 16). While this is much lower than the 8% observed in the IGLAD data, a higher prevalence of injuries to the heart compared to rib fractures is still implausible.

As a comparison to the results based on the empirical cumulative distribution derived in [20] (4.3 cases with one fractured rib and 0.1 cases with two fractured ribs), also the MPS of each individual rib was evaluated for all 75 simulations. For this, a threshold strain of 3% was chosen, which was used for the ribs of the THUMS v4 before [22] and is also equal to the weighted sum of the age-dependent thresholds (i.e. equivalent to a mean age of about 44 years). This method predicted no rib fractures. In only six of the 75 simulations, the MPS99 exceeded 2%, while the overall maximum value observed was 2.7%. The peak strains in all six simulations were located in the first left rib. If the threshold strain was lowered to 2%, which would be equivalent to an average age of 69 years in the sample, the method predicted six cases with a fractured rib. Assuming each of these single rib fractures would result in a hemo- or pneumothorax (which seems even less likely than a sample with an average age of 69 years), this would represent a relative frequency of AIS2+ injury of 8% and be identical to the relative frequency observed in the IGLAD sample. This was not implemented for the injury assessment based on the adjusted limits in Fig. 16 though, because the lower prevalence compared to the real-world data correlates well with the fact that only rib fractures and injuries to the heart were assessed. To this effect, the addition of other strain-based soft tissue injury metrics for the thorax, particularly for injury to the lungs, would be desirable in the future. While there is a growing body of literature on the issue [29–31], there are currently no robust injury metrics to distinguish between injured and non-injurious cases for the THUMS [32]. Based on rib fractures alone, the frequency of thoracic injuries seems to be underestimated in the simulations. Aside from the fact that soft tissue injury was not considered, there is a number of possible reasons for this. While the parameters for the restraint systems in the FE model were varied to account for the variability in the IGLAD sample, they were still based on state-of-the-art systems. It might be that the systems in the simulations still offer a more optimal occupant restraint than the systems in the real-world sample. In addition, the rib cage and the ribs themselves are subject to very large interpersonal variability [33] in terms of geometry and material properties. This diversity is also not accounted for in the present study, which used only one model and therefore one rib cage geometry.

The relative frequency of injuries to the neck, spine and lower extremity of the HBM matched the results observed in the IGLAD sample well. Injuries to the upper extremities were only predicted in 0.4% of cases, which is significantly lower than the 4.8% in the real-world accidents. Injuries to the neck, spine and upper extremities were only associated with cortical bone fracture. In addition, the lower extremities also included the separate strain assessment in the pelvic bones but the associated elements never exceeded their 1% strain limit. These skeletal parts of the THUMS are all modelled as having elasto-plastic properties and are validated for a number of component and whole body load cases [16]. While this HBM can be simulated with the option to model bone fractures directly, i.e. by eliminating elements which exceed a predefined failure strain during the simulation, this

was not chosen in the present study. Instead, fracture was assessed by means of strain thresholds in post-processing. While this has distinct benefits (improved numerical stability, possibility to assess fracture risk for different age groups), bone fractures could theoretically lead to penetrating injuries due to the resulting sharp bone edges or fragments, which was not considered. Since bone fracture was the only injury mechanism considered for these body regions and injuries which could be the consequence of a fractured bone were not accounted for, *lower* relative injury frequencies than those observed in real-world accidents are to be expected. Still, it is questionable, if a difference of about 4% for MAIS2+ upper extremity injuries can be explained by non-fracture injuries alone. One additional reason for this could be the hand positioning (see also Fig. A-6 and Fig. A-7). While positioning the HBM hands to grip the steering wheel could increase the injury risk for the upper extremities, hand positions in real-world cases might vary considerably.

Limitations

The present study has a number of limitations. Considering the accident analysis, it has to be noted that since the IGLAD sample only makes the MAIS value available for each body region, multiple injuries in one body region have not been accounted for. In addition, the representativeness of the accident data set was not tested specifically. Weighting could account for discrepancies between national statistics and case numbers in IGLAD [12]. Since the present study focussed only on passenger car drivers and because no general risks were calculated, no weighting was applied. Delta-v was chosen as a parameter to estimate collision severity. While this is common practice, the value itself, unless actually recorded during the collision by an event data recorder (EDR), is usually estimated in the accident reconstruction. In case of NASS-CDS, this estimation is known to have significant bias and scatter [8–9]. There are currently no similar studies available for IGLAD data, although at least similar scatter levels can be expected. Based on this, the known (and therefore unbiased) delta-v values in the simulations can be thought as being representative of a wider range of delta-v values if they were also based on estimations – like the real-world delta-v values.

Another limitation is the availability of representative crash loads themselves. In the present study, data from rigid wall crash test were used. While care was taken to create a simulation matrix with a similar range in terms of delta-v values, using data from real-world car-to-car collisions, i.e., by means actual pulses derived from EDR, could increase the value of the presented approach.

Several limitations concern the driver model. For the simulations with the FE HBM, only one anthropometry (THUMS v4.02 adult 50th percentile male) in one seated position was considered. Additional anthropometries, occupant positions and postures should be examined in the future. Particularly seat adjustments, which put the driver in a position closer to or further from the airbag have the potential to increase the injury risk in case of a crash. In a way, by neglecting these possible alterations, the simulation results represent a best-case scenario in terms of seat position. In addition, the HBM was passive, meaning that no muscle activity was considered. This could also lead to changes in the occupant-restraint-interaction, particularly in case of a distinct pre-crash phase, which would give the occupant a chance of reacting to an imminent collision. The positioning of the FE HBM in the seat was based on the position of a Hybrid III ATD. This method was chosen for reasons of simplicity; however, it must be noted that a human occupant would likely be seated differently than a crash test dummy. Since the seat position of the drivers in the real-world cases from the IGLAD database are unknown, *this* simplification was considered negligible.

Two other areas in which there are several limitations to be discussed are the vehicle model and the restraint systems. It must be noted that the current set of input parameters should be considered as one possible set. While these parameters produced the desired amount of variation and robust, plausible simulations, a different interior model might need a different set of input parameters. The airbag mass flow curve in the model used in this study was encrypted, which meant that the mass-flow could not be varied. In addition, the trigger times for each crash pulse had to be estimated. This is another region, where EDR data could be useful for future research in this area since it could provide real-life deployment times for the restraint systems. Since the times were subject to variation, the impact of not knowing the actual deployment times is expected to be negligible. It is important that the restraint systems available in the simulation reflect the probable fitment rates of the vehicles in the real-world data. To account for this in the present study, simulations with increased shoulder belt force limiter values or a deactivated knee airbag were conducted. While omitting the driver airbag could improve the representativeness for older vehicles further, this could also lead to problems with numerical stability when

simulating higher severity crashes. Therefore, variants excluding airbags were not simulated in the present study. While using only one interior and set of restraint systems can be seen as a limitation, this may also yield a potential benefit: The simulation matrix defined in this study can be seen as a set of virtual occupant safety load cases representative of real-world scenarios, which could be used to assess the safety performance of future interior concepts. In order to achieve this though, further research into the injury criteria and injury risk curves would be necessary.

Injury risk functions have to be calibrated to the specific HBM to which they are applied. Trend analysis based on real-world accidents, as implemented in the current study, can be used in addition to other sources. Furthermore, the approach shown in this paper can be used to estimate the outcome of varying simulation parameters and restraint systems relative to baseline results that should be in line with real-world injuries.

All simulation results in the current study were analysed with the open source software DYNASAUR [18] and MUTANT [19]. While this enables working with a large number of results at once in a time and resource efficient way, it also facilitates harmonisation and transparency of assessment procedures as well as the incorporation of new injury criteria and injury risk curves. Open source software and transparent injury assessment could be a key component towards standardised analysis methods of FE human body models.

V. CONCLUSIONS

This study used IGLAD data to investigate key injury regions of car drivers in frontal accidents. The results of this real-world accident data analysis are in accordance with similar studies, identifying the upper and lower extremities, the thorax and the head as key injury regions for MAIS2+ injuries. The filter criteria used for the IGLAD data were aimed to eliminate any cases with intrusion into the passenger compartment. This is why this analysis, unlike many other studies, found the upper extremities to be more frequently injured than the lower extremities. It also explains the lower prevalence of injuries to the lower extremities compared to the head and the thorax.

The attempt to replicate the relative injury frequency observed in real-world accidents with a FE HBM produced mixed results. While the relative prevalence of injuries to the spine and the lower extremities was matched well, the strain-based metrics for injuries to the brain and internal organs overestimated the frequency of injuries when compared to real-world data significantly. While the use of a model with state-of-the-art restraint systems would explain *lower* prevalence of injuries in the simulated cases, the results suggest that soft tissue injury metrics in particular are in need of improvement. Further research on injury risk curves for strain-based injury metrics is called for to improve the injury prediction of passenger car occupants. Ideally, these metrics should be non-proprietary to enable widespread application in research and industry alike.

Furthermore, when using a completely generic interior and restraint model, which can be parametrised to represent the interiors and restraints found in a large sample better, the results from the FE HBM could theoretically be used to argue thresholds and risk curves by matching the results to the accident analysis.

VI. ACKNOWLEDGEMENT

The authors would like to acknowledge the use of high performance computing resources provided by the IT Services (ZID) of Graz University of Technology. We would also like to thank the Toyota Motor Corporation and Toyota Central R&D Labs for providing the academic license of the THUMS v4.02 AM50 occupant model.

VII. REFERENCES

- [1] World Health Organization. (2018). Global status report on road safety 2018, Geneva.
- [2] Insurance Institute for Highway Safety "Fatality Facts 2018: Passenger vehicle occupants", <https://www.iihs.org/topics/fatality-statistics/detail/passenger-vehicle-occupants> [Accessed 17 February 2020].
- [3] Weaver A, Talton J, Barnard R, Schoell S, Swett K, Stitzel J. (2015) Estimated injury risk for specific injuries and body regions in frontal motor vehicle crashes. *Traffic Injury Prevention*, **16 Suppl 1**: pp.108–116.
- [4] Forman J, Poplin G, Shaw C, McMurry T, Schmidt K, Ash J *et al.* (2019) Automobile injury trends in the contemporary fleet: Belted occupants in frontal collisions. *Traffic Injury Prevention*, **20**(6): pp.607–612.
- [5] Carter P, Flannagan C, Reed M, Cunningham R, Rupp J. (2014) Comparing the effects of age, BMI and gender on severe injury (AIS 3+) in motor-vehicle crashes. *Accident Analysis & Prevention*, **72**: pp.146–160.
- [6] Golman A, Danelson K, Stitzel J. (2016) Robust human body model injury prediction in simulated side impact

- crashes. *Computer methods in biomechanics and biomedical engineering*, **19**(7): pp.717–732.
- [7] Golman A, Danelson K, Miller L, Stitzel J. (2014) Injury prediction in a side impact crash using human body model simulation. *Accident Analysis & Prevention*, **64**: pp.1–8.
- [8] Iraeus J "Stochastic finite element simulations of real life frontal crashes": *With emphasis on chest injury mechanisms in near-side oblique loading conditions*, Umeå.
- [9] Iraeus J, Lindquist M Development and validation of a generic finite element vehicle buck model for the analysis of driver rib fractures in real life nearside oblique frontal crashes. In: *Accident Analysis & Prevention* 952016. pp. 42–56.
- [10] Li G, Otte D, Yang J, Simms C. (2016) Can a Small Number of Pedestrian Impact Scenarios Represent the Range of Real-world Pedestrian Injuries? *Proceedings of IRCOBI Conference, 2016, Malaga, Spain*.
- [11] IGLAD Technical Working Group. (2018). IGLAD Codebook,
- [12] Bakker J, Jeppson H, Hannawald L, Spitzhüttel F, Longton A, Tomasch E. (2017) IGLAD - International Harmonized In-Depth Accident Data. *Proceedings of International Technical Conference on the Enhanced Safety of Vehicles, 2017, Michigan, USA*.
- [13] SAE International "Collision Deformation Classification", Recommended Practice J224, 400 Commonwealth Drive, Warrendale, PA, United States.
- [14] Association for the Advancement of Automotive Medicine. (2008). Abbreviated Injury Scale 2005 Update 2008, pp.175, Barrington, IL, US.
- [15] National Highway Traffic Safety Administration "NHTSA VSR | NHTSA vehicle Crash Test Database", <https://www-nrd.nhtsa.dot.gov/database/veh/veh.htm> [Accessed 17 February 2020].
- [16] Toyota Motor Corporation. (2015). Documentation Total Human Model for Safety (THUMS), pp.74.
- [17] National Highway Traffic Safety Administration. (2008). FMVSS Test Procedure 208-14 - Appendix F: Dummy Positioning Procedures for Driver and Passenger Test Dummy Conforming to Subpart E of Part 572,
- [18] Klug C, Luttenberger P, Schachner M, Micorek J, Greimel R, Sinz W. (2018) Postprocessing of Human Body Model Results – Introduction of the Open Source Tool DYNASAUR. *Proceedings of 7th International Symposium: Human Modeling and Simulation in Automotive Engineering, 2018, Berlin, Germany*.
- [19] Luttenberger P, Schachner M, Rajinovic S, Moser J, Leo C, Sinz W. (2019). MUTANT Functionality Report, Graz.
- [20] Forman J, Kent R, Mroz K, Pipkorn B, Bostrom O, Segui-Gomez M. (2012) Predicting Rib Fracture Risk with Whole-Body Finite Element Models: Development and Preliminary Evaluation of a Probabilistic Analytical Framework. *Annals of Advances in Automotive Medicine*, **56**: pp.109–124.
- [21] Association for the Advancement of Automotive Medicine. (1998). Abbreviated Injury Scale; 1990 Revision: Update 98. AAAM, Barrington, IL, US.
- [22] Watanabe R, Miyazaki H, Kitagawa Y, Yasuki T. (2011) Research of the Relationship of Pedestrian Injury to Collision Speed, Car-type, Impact Location and Pedestrian Sizes Using Human FE Model (THUMS Version 4). *Proceedings of International Technical Conference on the Enhanced Safety of Vehicles, 2011, Washington, D.C., USA*.
- [23] Snedeker J, Muser M, Walz F. (2003) Assessment of pelvis and upper leg injury risk in car-pedestrian collisions: comparison of accident statistics, impactor tests and a human body finite element model. *Stapp Car Crash Journal*, **47**: pp.437–457.
- [24] Laituri T, Henry S, Pline K, Li G, Frankstein M, Weerappuli P. (2016) New Risk Curves for NHTSA's Brain Injury Criterion (BrIC): Derivations and Assessments. *Stapp Car Crash Journal*, **60**: pp.1–64.
- [25] Takhounts E, Craig M, Moorhouse K, McFadden J, Hasija V. (2013) Development of brain injury criteria (BrIC). *Stapp Car Crash Journal*, **57**: pp.243–266.
- [26] Takhounts E, Hasija V, Craig M. (2019) BrIC and Field Brain Injury Risk. *Proceedings of International Technical Conference on the Enhanced Safety of Vehicles, 2019, Eindhoven, Netherlands*.
- [27] Liangliang Shi, Yong Han, Hongwu Huang, Johan Davidsson, Robert Thomson Evaluation of injury thresholds for predicting severe head injuries in vulnerable road users resulting from ground impact via detailed accident reconstructions. *Biomechanics and Modeling in Mechanobiology*: pp.1–19.
- [28] Wang F, Han Y, Wang B, Peng Q, Huang X, Miller K *et al.* (2018) Prediction of brain deformations and risk of traumatic brain injury due to closed-head impact: quantitative analysis of the effects of boundary conditions and brain tissue constitutive model. *Biomechanics and Modeling in Mechanobiology*, **17**(4): pp.1165–1185.

[29] Stitzel J, Gayzik F, Hoth J, Mercier J, Gage H, Morton K *et al.* (2005) Development of a finite element-based injury metric for pulmonary contusion part I: model development and validation. *Stapp Car Crash Journal*, **49**: pp.271–289.

[30] Gayzik F, Hoth J, Daly M, Meredith J, Stitzel J. (2007) A finite element-based injury metric for pulmonary contusion: investigation of candidate metrics through correlation with computed tomography. *Stapp Car Crash Journal*, **51**: pp.189–209.

[31] Gayzik F, Hoth J, Stitzel J. (2011) Finite element-based injury metrics for pulmonary contusion via concurrent model optimization. *Biomechanics and Modeling in Mechanobiology*, **10**(4): pp.505–520.

[32] Gaewsky J, Weaver A, Stitzel J. (2017) A Numerical Approach to Identify Injury Risk Regions within Soft Tissues of Dynamic Human Body Finite Element Models. *Proceedings of International Technical Conference on the Enhanced Safety of Vehicles*, 2017, Michigan, USA.

[33] Iraeus J, Pipkorn B. (2019) Development and Validation of a Generic Finite Element Ribcage to be used for Strain-based Fracture Prediction. *Proceedings of IRCOBI Conference*, 2019, Florence, Italy.

VIII. APPENDIX

Filters applied to the IGLAD sample

The filters were set to only include

- cases with male drivers of passenger cars
- frontal accidents (i.e. main area of deformation: front, primary direction of force: 0°)
- cases with known delta-v between 28 km/h and 64 km/h

while excluding

- cases where the belt was not used or misused
- cases with secondary collisions
- collisions with vulnerable road users, animals and cases in which the opponent had not been specified
- cases with implausible data (in five cases two delta-v values but only one collision was coded)
- cases with deformation into the passenger compartment (filter set to exclude CDC deformation extent > 5 or unknown)
- small overlap crashes (filter set to exclude CDC specific longitudinal location of deformation codes L0 and R0).



Fig. A-1. Source countries of the accidents in the IGLAD sample for male car drivers in frontal collisions with delta-v 28 - 64 km/h (n=124). Additional filters are listed above.



Fig. A-2. Source countries of the accidents in the unfiltered IGLAD sample (n=4,943). It can be seen that the sample distribution in Fig. A-1 is very similar.

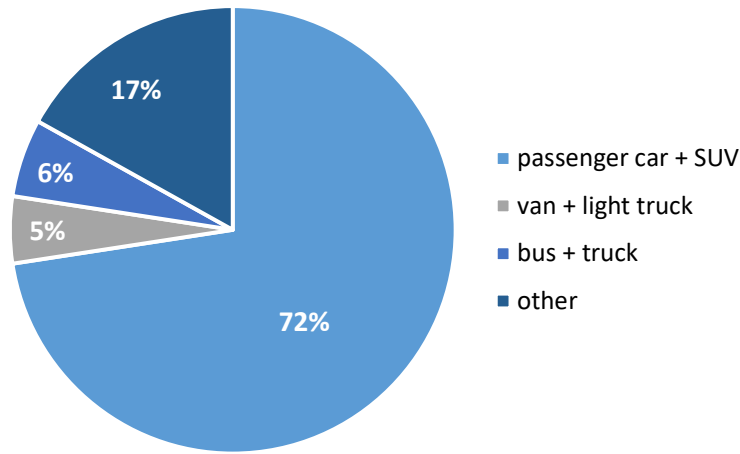


Fig. A-3. Distribution of collision opponents in the IGLAD sample for male car drivers in frontal collisions with delta-v 28 - 64 km/h (n=124). Additional filters are listed above.

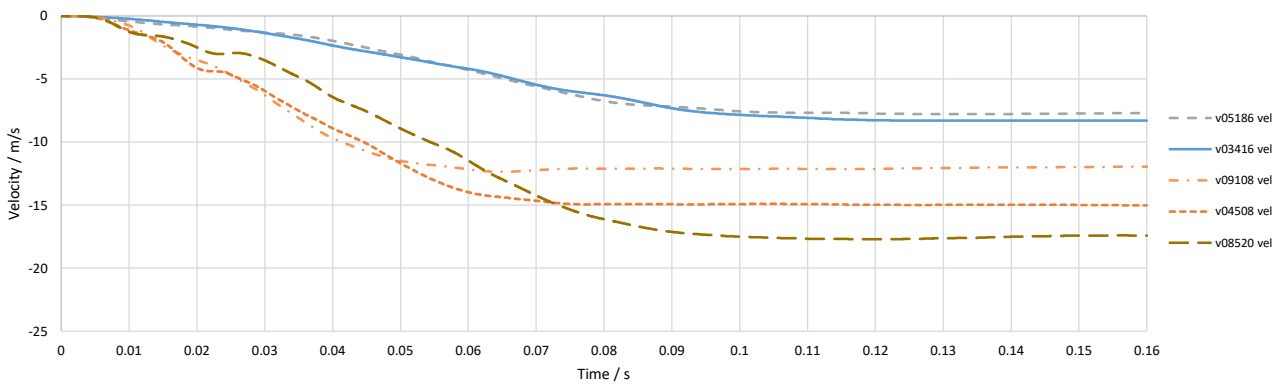


Fig. A-4. Velocity time-history curves of the crash pulses extracted from full overlap rigid wall crash test data in the NHTSA VSR database [15].

Note: The curves plotted here start at the axis system’s origin. In the individual simulations, they are offset according to their initial velocity (listed in the simulation matrix in Table A-II).

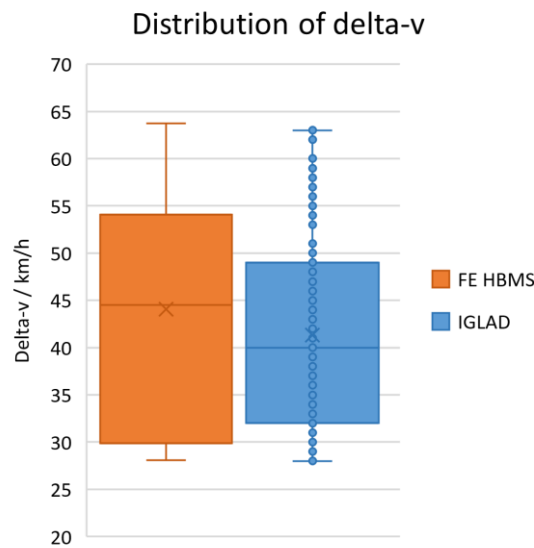


Fig. A-5. Box plots of delta-v for the IGLAD sample and the FE HBM simulations. The mean delta-v values for the FE HBM simulations and the IGLAD sample are 44.1 km/h and 41.3 km/h respectively.



Fig. A-6. View of hand position next to the steering wheel in Y-Z plane.

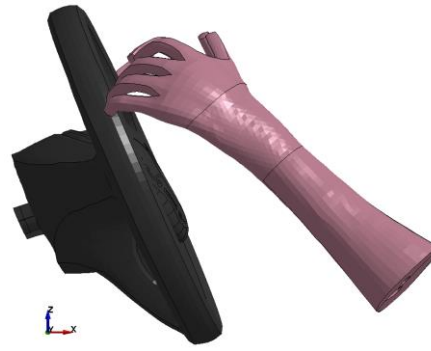


Fig. A-7. View of hand position next to the steering wheel in X-Z plane.

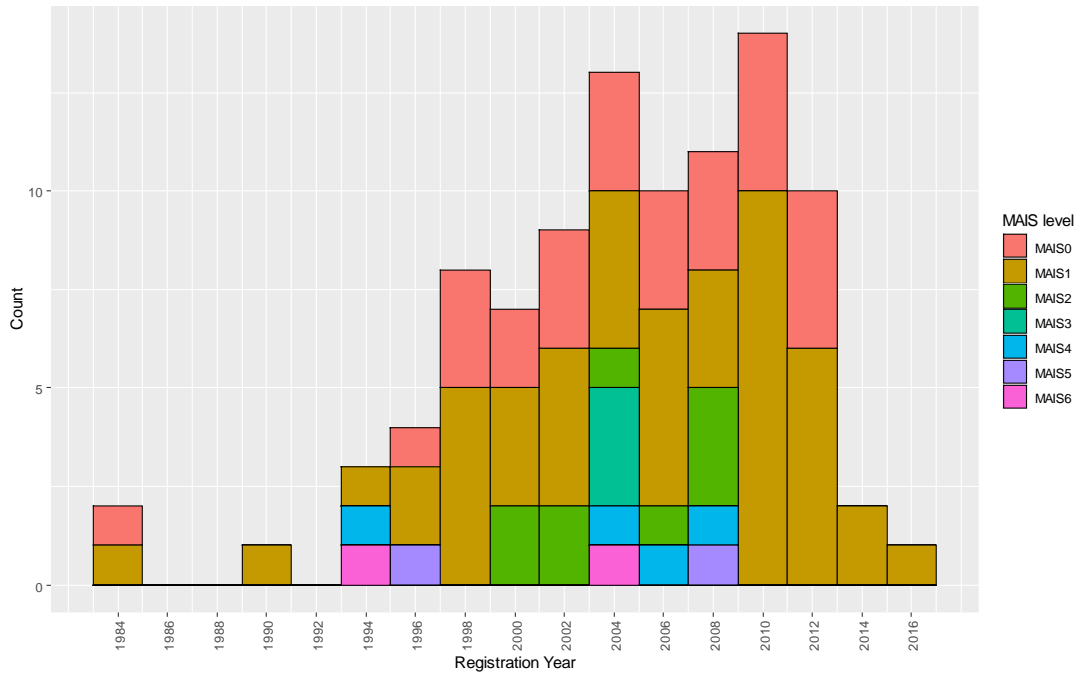


Fig. A-8. Histogram of vehicle registration year in the IGLAD data (n = 118).

Deployment Algorithm

The longitudinal acceleration signal has been monitored until a deceleration threshold of 9.81 ms^{-2} (or 1 g) was exceeded. From this point in time, the acceleration signal was integrated twice to obtain the distance travelled during the crash. The deployment was triggered, as soon as this cumulative distance value exceeded three millimetres. This algorithm was checked against Case No. 9,725 in the NHTSA database, which also includes time history files for the airbag trip switch. The TTF according to the algorithm is 10.38 ms, which matches the 10.0 ms observed in the sensor data well. Deployment times for all crash pulses were determined in this way and are listed in Table A-II.

n = 124	SUM	HEAD	FACE	NECK	THORAX	ABDOMEN	SPINE	UX	LX	UNKNOWN
MAIS0	792	89	91	102	61	101	92	72	79	105
MAIS1	133	4	16	6	29	6	13	31	25	3
MAIS2	22	3	1	1	5	1	4	6	1	0
MAIS3	5	0	0	0	2	0	0	0	3	0
MAIS4	4	3	0	0	0	0	0	0	1	0
MAIS5	4	0	0	0	3	1	0	0	0	0
MAIS6	2	1	0	0	0	0	0	0	0	1
unknown	154	24	16	15	24	15	15	15	15	15

Fig. A-9. Number of MAIS0 to MAIS6 injuries for each body region based on the IGLAD sample when filtering for male car drivers in frontal collisions with delta-v 28 - 64 km/h.

n = 124	SUM	HEAD	FACE	NECK	THORAX	ABDOMEN	SPINE	UX	LX	UNKNOWN
MAIS0	71%	72%	73%	82%	49%	81%	74%	58%	64%	85%
MAIS1+	15%	9%	14%	6%	31%	6%	14%	30%	24%	3%
MAIS2+	3%	6%	1%	1%	8%	2%	3%	5%	4%	1%
MAIS3+	1%	3%	0%	0%	4%	1%	0%	0%	3%	1%
MAIS4+	1%	3%	0%	0%	2%	1%	0%	0%	1%	1%
MAIS5+	1%	1%	0%	0%	2%	1%	0%	0%	0%	1%
MAIS6	0%	1%	0%	0%	0%	0%	0%	0%	0%	1%
unknown	14%	19%	13%	12%	19%	12%	12%	12%	12%	12%

Fig. A-10. Relative injury frequency for each body region with respect to MAISx+ injury severity in percentage based on the IGLAD sample when filtering for male car drivers in frontal collisions with delta-v 28 - 64 km/h.

TABLE A-I
SIMULATED VARIANTS

Var.	PDOF [°]	Fb3 [kN]	Col. Force [kN]	SLL	KAB	Vent Dia. [mm]	μ _{AB}	ΔTTF [ms]	Description
1	0	3.8	4.2	0	1	35	0.4	0	baseline - executive saloon
2	+15	3.8	4.2	0	1	35	0.4	0	+15°
3	-15	3.8	4.2	0	1	35	0.4	0	-15°
4	0	3.8	4.2	0	0	35	0.4	0	lower spec (no KAB)
5	0	5.0	4.2	1	1	35	0.4	0	higher spec (SLL): higher shoulder belt force, second load limiter
6	0	6.0	4.2	0	1	35	0.4	0	older vehicle: higher shoulder belt force
7	0	6.0	4.2	0	1	35	0.1	0	older vehicle (variation): higher shoulder belt force, lower AB friction
8	0	3.8	4.2	0	1	35	0.4	-3	fast trigger: TTF variation
9	0	3.8	4.2	0	1	25	0.4	+5	older vehicle: stiffer AB, later TTF
10	0	4.5	4.2	0	1	35	0.4	+5	older vehicle: higher shoulder belt force, later TTF
11	0	6.0	3.8	0	1	50	0.4	0	more belt loading: softer steering column, softer AB, higher shoulder belt force, lower AB friction
12	0	6.0	3.8	0	1	50	0.1	0	more belt loading: softer steering column, softer AB, higher shoulder belt force
13	0	4.5	3.8	0	1	50	0.4	+5	more belt loading: softer steering column, softer AB, higher shoulder belt force, later TTF
14	0	5.0	4.8	0	1	35	0.4	+5	older vehicle: slightly stiffer steering column, higher shoulder belt force, later TTF
15	0	3.8	6.0	0	1	35	0.4	0	older vehicle: stiffer steering column

These 15 variants were simulated for all five crash pulses. This was the basis for the simulation matrix (listed in Table A-II).

TABLE A-II
SIMULATION MATRIX OF THE FE SIMULATIONS

ID	No.	NHTSA-ID	initial_vel	forceLimit retractor	forceLimit steerCol	TTF_SRet	TTF_PRet	TTS_LL2	TTF_DAB	TTF_KAB	VENT	delta-v	μ _{AB}	deltaTTF
054-T450-p9100016-noY	054	03416	6.67	3.8	4.2	12.85	17.85	200.0	17.85	17.85	35	29.89	0.40	-3
055-T450-p9100018-noY	055	05186	6.56	3.8	4.2	10.15	15.15	200.0	15.15	15.15	35	28.09	0.40	-3
067-T450-p9100011-noY	067	08520	15.57	3.8	4.2	9.77	14.77	200.0	14.77	14.77	35	63.73	0.40	0
068-T450-p9100011-noY	068	08520	15.57	5.0	4.8	14.77	19.77	200.0	19.77	19.77	35	63.73	0.40	5
071-T450-p9100016-noY	071	03416	6.67	3.8	4.2	15.85	20.85	200.0	20.85	20.85	35	29.89	0.40	0
072-T450-p9100016-noY	072	03416	6.67	5.0	4.8	20.85	25.85	200.0	25.85	25.85	35	29.89	0.40	5
073-T450-p9100017-noY	073	04508	13.27	3.8	4.2	9.81	14.81	200.0	14.81	14.81	35	54.05	0.40	0
074-T450-p9100017-noY	074	04508	13.27	5.0	4.8	14.81	19.81	200.0	19.81	19.81	35	54.05	0.40	5
075-T450-p9100018-noY	075	05186	6.56	3.8	4.2	13.15	18.15	200.0	18.15	18.15	35	28.09	0.40	0
076-T450-p9100018-noY	076	05186	6.56	5.0	4.8	18.15	23.15	200.0	23.15	23.15	35	28.09	0.40	5
079-T450-p9100011-noY	079	08520	15.57	3.8	4.2	9.77	14.77	200.0	14.77	200	35	63.73	0.40	0
083-T450-p9100016-noY	083	03416	6.67	3.8	4.2	15.85	20.85	200.0	20.85	200	35	29.89	0.40	0
085-T450-p9100017-noY	085	04508	13.27	3.8	4.2	9.81	14.81	200.0	14.81	200	35	54.05	0.40	0
087-T450-p9100018-noY	087	05186	6.56	3.8	4.2	13.15	18.15	200.0	18.15	200	35	28.09	0.40	0
092-T450-p9100011-noY	092	08520	15.57	4.5	4.2	14.77	19.77	200.0	19.77	19.77	35	63.73	0.40	5
093-T450-p9100011-noY	093	08520	15.57	6.0	4.2	9.77	14.77	200.0	14.77	14.77	35	63.73	0.40	0
094-T450-p9100011-noY	094	08520	15.57	6.0	4.2	9.77	14.77	200.0	14.77	14.77	35	63.73	0.1	0
098-T450-p9100016-noY	098	03416	6.67	4.5	4.2	20.85	25.85	200.0	25.85	25.85	35	29.89	0.40	5
099-T450-p9100016-noY	099	03416	6.67	6.0	4.2	15.85	20.85	200.0	20.85	20.85	35	29.89	0.40	0
100-T450-p9100016-noY	100	03416	6.67	6.0	4.2	15.85	20.85	200.0	20.85	20.85	35	29.89	0.1	0
101-T450-p9100017-noY	101	04508	13.27	4.5	4.2	14.81	19.81	200.0	19.81	19.81	35	54.05	0.40	5
102-T450-p9100017-noY	102	04508	13.27	6.0	4.2	9.81	14.81	200.0	14.81	14.81	35	54.05	0.40	0
103-T450-p9100017-noY	103	04508	13.27	6.0	4.2	9.81	14.81	200.0	14.81	14.81	35	54.05	0.1	0
104-T450-p9100018-noY	104	05186	6.56	4.5	4.2	18.15	23.15	200.0	23.15	23.15	35	28.09	0.40	5
105-T450-p9100018-noY	105	05186	6.56	6.0	4.2	13.15	18.15	200.0	18.15	18.15	35	28.09	0.40	0
106-T450-p9100018-noY	106	05186	6.56	6.0	4.2	13.15	18.15	200.0	18.15	18.15	35	28.09	0.1	0
107-T450-p9100024-noY	107	09108	11.06	4.5	4.2	16.11	21.11	200.0	21.11	21.11	35	44.53	0.40	5
108-T450-p9100024-noY	108	09108	11.06	6.0	4.2	11.11	16.11	200.0	16.11	16.11	35	44.53	0.40	0
109-T450-p9100024-noY	109	09108	11.06	6.0	4.2	11.11	16.11	200.0	16.11	16.11	35	44.53	0.1	0
113-T450-p9100011-noY	113	08520	15.57	4.5	3.8	14.77	19.77	200.0	19.77	19.77	50	63.73	0.40	5
114-T450-p9100011-noY	114	08520	15.57	6.0	3.8	9.77	14.77	200.0	14.77	14.77	50	63.73	0.40	0
115-T450-p9100011-noY	115	08520	15.57	6.0	3.8	9.77	14.77	200.0	14.77	14.77	50	63.73	0.1	0
119-T450-p9100016-noY	119	03416	6.67	4.5	3.8	20.85	25.85	200.0	25.85	25.85	50	29.89	0.40	5
120-T450-p9100016-noY	120	03416	6.67	6.0	3.8	15.85	20.85	200.0	20.85	20.85	50	29.89	0.40	0
121-T450-p9100016-noY	121	03416	6.67	6.0	3.8	15.85	20.85	200.0	20.85	20.85	50	29.89	0.1	0
122-T450-p9100017-noY	122	04508	13.27	4.5	3.8	14.81	19.81	200.0	19.81	19.81	50	54.05	0.40	5
123-T450-p9100017-noY	123	04508	13.27	6.0	3.8	9.81	14.81	200.0	14.81	14.81	50	54.05	0.40	0
124-T450-p9100017-noY	124	04508	13.27	6.0	3.8	9.81	14.81	200.0	14.81	14.81	50	54.05	0.1	0
125-T450-p9100018-noY	125	05186	6.56	4.5	3.8	18.15	23.15	200.0	23.15	23.15	50	28.09	0.40	5
126-T450-p9100018-noY	126	05186	6.56	6.0	3.8	13.15	18.15	200.0	18.15	18.15	50	28.09	0.40	0
127-T450-p9100018-noY	127	05186	6.56	6.0	3.8	13.15	18.15	200.0	18.15	18.15	50	28.09	0.1	0
128-T450-p9100024-noY	128	09108	11.06	4.5	3.8	16.11	21.11	200.0	21.11	21.11	50	44.53	0.40	5
129-T450-p9100024-noY	129	09108	11.06	6.0	3.8	11.11	16.11	200.0	16.11	16.11	50	44.53	0.40	0
130-T450-p9100024-noY	130	09108	11.06	6.0	3.8	11.11	16.11	200.0	16.11	16.11	50	44.53	0.1	0
131-T450-p9100011-noY	131	08520	15.57	3.8	4.2	6.77	11.77	200.0	11.77	11.77	35	63.73	0.40	-3
133-T450-p9100017-noY	133	04508	13.27	3.8	4.2	6.81	11.81	200.0	11.81	11.81	35	54.05	0.40	-3
134-T450-p9100024-noY	134	09108	11.06	3.8	4.2	8.11	13.11	200.0	13.11	13.11	35	44.53	0.40	-3
135-T450-p9100024-noY	135	09108	11.06	4.2	11.11	16.11	200.0	16.11	200	35	44.53	0.40	0	
136-T450-p9100024-noY	136	09108	11.06	5.0	4.8	16.11	21.11	200.0	21.11	21.11	35	44.53	0.40	5
137-T450-p9100024-noY	137	09108	11.06	3.8	4.2	11.11	16.11	200.0	16.11	16.11	35	44.53	0.40	0
139-T450-p9100011-noY	139	08520	15.57	5.0	4.2	9.77	14.77	39.77	14.77	14.77	35	63.73	0.40	0
141-T450-p9100016-noY	141	03416	6.67	5.0	4.2	15.85	20.85	45.85	20.85	20.85	35	29.89	0.40	0
142-T450-p9100017-noY	142	04508	13.27	5.0	4.2	9.81	14.81	39.81	14.81	14.81	35	54.05	0.40	0
143-T450-p9100018-noY	143	05186	6.56	4.0	4.2	13.15	18.15	43.15	18.15	18.15	35	28.09	0.40	0
144-T450-p9100024-noY	144	09108	11.06	5.0	4.2	11.11	16.11	41.11	16.11	16.11	35	44.53	0.40	0
146-T450-p9100011-noY	146	08520	15.57	3.8	6.0	9.77	14.77	200.0	14.77	14.77	35	63.73	0.40	0
148-T450-p9100016-noY	148	03416	6.67	3.8	6.0	15.85	20.85	200.0	20.85	20.85	35	29.89	0.40	0
149-T450-p9100017-noY	149	04508	13.27	3.8	6.0	9.81	14.81	200.0	14.81	14.81	35	54.05	0.40	0
150-T450-p9100018-noY	150	05186	6.56	3.8	6.0	13.15	18.15	200.0	18.15	18.15	35	28.09	0.40	0
151-T450-p9100024-noY	151	09108	11.06	3.8	6.0	11.11	16.11	200.0	16.11	16.11	35	44.53	0.40	0
153-T450-p9100011-noY	153	08520	15.57	3.8	4.2	14.77	19.77	200.0	19.77	19.77	25	63.73	0.40	5
155-T450-p9100016-noY	155	03416	6.67	3.8	4.2	20.85	25.85	200.0	25.85	25.85	25	29.89	0.40	5
156-T450-p9100017-noY	156	04508	13.27	3.8	4.2	14.81	19.81	200.0	19.81	19.81	25	54.05	0.40	5
157-T450-p9100018-noY	157	05186	6.56	3.8	4.2	18.15	23.15	200.0	23.15	23.15	25	28.09	0.40	5
158-T450-p9100024-noY	158	09108	11.06	3.8	4.2	16.11	21.11	200.0	21.11	21.11	25	44.53	0.40	5
185-T450-p9100118-riY	185	05186x	6.56	3.8	4.2	13.15	18.15	200.0	18.15	18.15	35	28.09	0.40	0
186-T450-p9100116-riY	186	03416x	6.67	3.8	4.2	15.85	20.85	200.0	20.85	20.85	35	29.89	0.40	0
187-T450-p9100124-riY	187	09108x	11.06	3.8	4.2	11.11	16.11	200.0	16.11	16.11	35	44.53	0.40	0
188-T450-p9100117-riY	188	04508x	13.27	3.8	4.2	9.81	14.81	200.0	14.81	14.81	35	54.05	0.40	0
189-T450-p9100111-riY	189	08520x	15.57	3.8	4.2	9.77	14.77	200.0	14.77	14.77	35	63.73	0.40	0
191-T450-p9100118-leY	191	05186x	6.56	3.8	4.2	13.15	18.15	200.0	18.15	18.15	35	28.09	0.40	0
192-T450-p9100116-leY	192	03416x	6.67	3.8	4.2	15.85	20.85	200.0	20.85	20.85	35	29.89	0.40	0
193-T450-p9100124-leY	193	09108x	11.06	3.8	4.2	11.11	16.11	200.0	16.11	16.11	35	44.53	0.40	0
194-T450-p9100117-leY	194	04508x	13.27	3.8	4.2	9.81	14.81	200.0	14.81	14.81	35	54.05	0.40	0
195-T450-p9100111-leY	195	08520x	15.57	3.8	4.2	9.77	14.77	200.0	14.77	14.77	35	63.73	0.40	0